Submitted to the International Europhysics Conference on High Energy Physics,
HEP97, Jerusalem, Israel, August 1997

Multiplicity Structure of Hadronic Final States in Diffractive Deep-Inelastic Scattering at HERA

H1 Collaboration

Abstract

The charged particle multiplicity of the hadronic system X in deep-inelastic processes at HERA of the form $ep \to eXY$, where Y is either a proton or a system with mass less than 1.6 GeV, is studied as a function of the invariant mass M_X of the system X. Results for multiplicity moments, correlations between forward and backward hemispheres in the rest frame of X and the multiplicity distribution itself, in various rapidity domains, are compared to data from e^+e^- annihilations, lepton-hadron and hadron-hadron collisions and to Monte Carlo models. Evidence is presented to show that the hadronic final state in diffractive DIS is more complex than the final state resulting from the fragmentation of a single colour string or from multi-string configurations as in hadron-hadron collisions. The results presented are well reproduced by gluon-dominated models for diffraction.

Abstract EPS-0250
Parallel Sessions 2,3,4
Plenary Sessions 1,2

1 Introduction

In deep-inelastic ep scattering (DIS) at HERA, a class of events is observed characterized by a large (pseudo-)rapidity gap (LRG) between the direction of the proton beam and the first significant energy deposit in the main detector [1,2]. The existence of the gap is a signal for the suppression of colour flow between the struck proton and the partonic fragments of the current. This indicates that the interaction is mediated by the exchange of a colourless state or proceeds as if the virtual photon (γ^*) effectively interacts with a soft, colour-neutral component of the proton. The LRG events are attributed mainly to diffraction or, in the language of Regge theory, to pomeron ($I\!P$) exchange [3,4].

The topology and kinematics of the LRG events can be discussed quite generally in terms of the process $ep \to eXY$ (see Fig. 1), where the hadronic systems X and Y are separated by the largest rapidity gap in the event. In the H1 experiment, events with no activity in a large pseudo-rapidity domain adjacent to the outgoing proton beam are selected. In these events the beam proton either stays intact (Y = proton in Fig. 1), or is excited to a low-mass baryonic system by a colourless exchange. The virtual photon, ranging from very low to very high virtuality, can be excited into a vector meson ($\gamma^* + p \to VM + p'$), or dissociate into a high mass state X ($\gamma^* + p \to X + p'$).

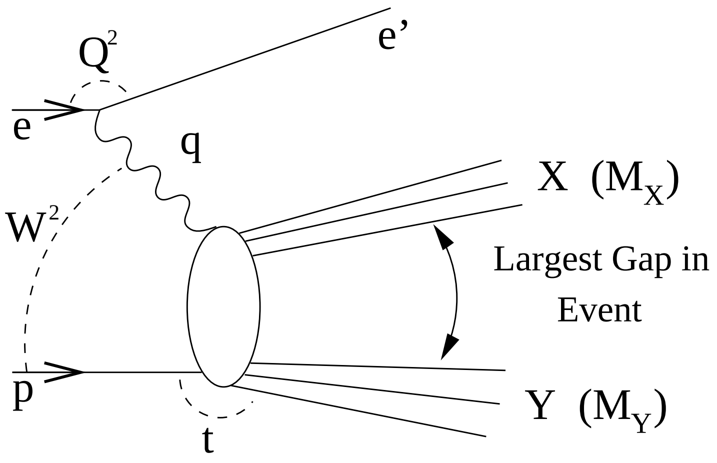

Figure 1: Illustration of the generic process, $ep \to eXY$ in which X and Y are separated by the largest rapidity gap in the event.

In this paper, first results are presented on charged particle density, multiplicity distributions and forward-backward multiplicity correlations measured in the centre-of-mass (CMS) of the particle system X, with invariant mass M_X, predominantly produced via diffractive dissociation of the virtual photon. In this frame, the virtual photon direction defines the positive z-axis.

At the small values of Bjorken-x (x) attainable at HERA, the diffractively produced final states X are expected to be sensitive to the topology and colour structure of partonic fluctuations of the virtual photon [5–9]. The data will, for that reason, be compared with data from e^+e^-, lepton-nucleon and hadron-hadron collisions. In e^+e^- annihilations with CMS energies, $\sqrt{s}$, in the range of M_X studied here, the partonic final state consist dominantly of a single quark-antiquark ($q\bar{q}$) pair connected by a colour flux-tube or string. In fixed target DIS, a single quark-diquark configuration dominates for the equivalent energy range in W. In hadron-hadron collisions, on the contrary, multi-string effects are known to be important.

A comparison of all these processes should reveal to which extent differences in primary partonic and colour structure can be discerned on the basis of the hadronic fragmentation products.

The data will also be compared to Monte Carlo models. Popular parton-model pictures of diffraction used in Monte Carlo simulations range from so-called quark dominated pomeron processes (see Fig. 2a), which lead to a final state parton configuration composed dominantly of a single quark-antiquark pair, to gluon dominated pomeron processes (Fig. 2b), which have a more complex partonic configuration and colour topology.

2 Experimental procedure

2.1 The experiment

The experiment was carried out with the H1 detector [10] at the HERA storage ring in DESY. The data were collected during the 1994 running period when 27.6 GeV positrons collided with 820 GeV protons, at a centre of mass energy of 300 GeV. The following briefly describes the detector components most relevant to this analysis.

The energy of the scattered positron is measured with a backward electromagnetic lead-scintillator calorimeter (BEMC), extending over the polar angular range $151^\circ < \theta < 177^\circ$ with full azimuthal coverage. The electromagnetic energy resolution of the BEMC is $\sigma_E/E \approx 0.10/\sqrt{E[\mathrm{GeV}]} \oplus 0.42/E[\mathrm{GeV}] \oplus 0.03$, while the BEMC energy scale for positrons is known to an accuracy of 1% [11]. A backward proportional chamber (BPC), situated immediately in front of the BEMC and with an angular acceptance of $155.5^\circ < \theta < 174.5^\circ$, serves to measure the impact point of the scattered positron and to confirm that the particle entering the BEMC is charged. Using information from the BPC, the BEMC and the reconstructed event vertex, the polar angle of the scattered positron can be determined to better than 1 mrad.

The hadronic final state is measured by tracking detectors surrounded by calorimeters. The central tracking detectors are a hybrid of inner and outer cylindrical jet chambers, z-drift chambers and proportional chambers. The jet chambers, mounted concentrically around the beam line, inside a homogeneous magnetic field of 1.15 Tesla, provide particle charge and momentum from track curvature and cover the angular interval $15^\circ < \theta < 165^\circ$. Up to 56 space points can be measured for non-curling tracks. The liquid argon calorimeter (LAr) extends over the polar angular range $4^\circ < \theta < 154^\circ$ with full azimuthal coverage. The LAr hadronic energy resolution is $\sigma_E/E \approx 0.50/\sqrt{E[\mathrm{GeV}]} \oplus 0.02$ as determined in test beams [12]. A study of the transverse momentum balance between the hadronic final state and the scattered positron, $p_T^{hadr}/p_T^{e'}$, has shown that the absolute hadronic energy scale is known to an accuracy of 4%. Backward going hadrons can be detected by the BEMC. The hadronic energy scale of the BEMC is known to a precision of 20%.

Forward energy at small angles is observed in several detectors near the outgoing proton beam direction. Particles reach these detectors both directly from the interaction point and indirectly as a result of secondary scattering with the beam pipe wall or adjacent material like collimators. The detectors are thus sensitive to energy coming from directions beyond their geometrical acceptances. The effective ranges of sensitivity to energy flow are $\eta \lesssim 5.5$ for the LAr, $3.5 \lesssim \eta \lesssim 5.5$ for the copper/silicon sandwich 'plug' calorimeter, $4.5 \lesssim \eta \lesssim 6.5$ for the forward muon spectrometer and $6.0 \lesssim \eta \lesssim 7.5$ for the proton remnant tagger, a lead-scintillator calorimeter located 24 m from the interaction point. These detectors overlap considerably in their rapidity coverage, thereby allowing for intercalibration of their efficiencies.

2.2 Monte Carlo models

Monte Carlo simulations are used in this analysis to apply acceptance and efficiency corrections to the observed data and to produce predictions for the hadronic final state that correspond to underlying parton models as shown in Fig. 2.

These simulations use the RAPGAP generator [13], which models deep-inelastic scattering of (virtual) photons off the pomeron or reggeon. The pomeron and reggeon fluxes inside the proton are taken form Regge theory. The pomeron is further assumed to have a partonic content which was evaluated from a QCD analysis of the measured diffractive structure function [14], using the DGLAP evolution equations, and is dominated by hard gluons. For the reggeon the GRV parametrisation of the pion structure function [15] is used. The underlying partonic processes considered in RAPGAP are shown in Fig. 2. The diagrams with a gluon in the partonic final state are of order α_S, but the relative contributions of the different diagrams are further controled by the quark and gluon content of the exchanged object. Fragmentation is provided either by the colour dipole model as implemented in ARIADNE [16] or parton showers as implemented in LEPTO [17] with subsequent string hadronisation as implemented in JETSET [18]. QED radiative processes are included via an interface to the program HERACLES [19].

2.3 Event and track selection

A neutral current DIS event selection is made by demanding a well-reconstructed scattered positron detected in the BEMC with an energy, E'_e, larger than 10 GeV. The efficiency of the BEMC trigger for positron energies larger than 10 GeV is known to be better than 99%. A subsample of dominantly diffractive events is then selected by requiring no activity above noise levels in any of the forward detectors or in the most forward part ($\eta > 3.2$) of the LAr Calorimeter.

Further cuts are applied to ensure a good quality reconstructed positron. An event vertex, reconstructed from tracks in the central trackers, within ± 30 cm of the mean vertex position, is required to reject beam-induced background. Events with coherent noise in the calorimeter or

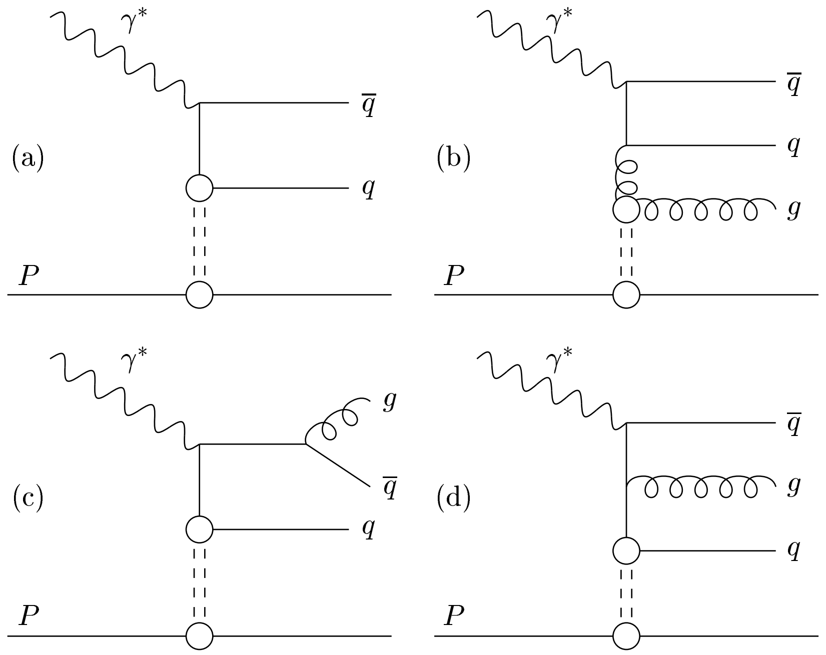

Figure 2: Underlying parton processes implemented in RAPGAP: (a) shows the lowest order process; the boson-gluon fusion (b) and QCD Compton (c,d) diagrams are of order α_S.

with a time-of-flight veto from the scintillator hodoscope are rejected.

The deep-inelastic kinematic variables (y_{Bj}, Q^2) are reconstructed using information from the scattered positron. The diffractive kinematic variables ($x_{I\!P}, M_X$) [1] are calculated from a combination of tracks and energy clusters, observed by the Central Tracker and the LAr Calorimeter [14].

The data are restricted and corrected to a kinematic region where the acceptance of the H1 detector is high and the contribution from background processes is low. Together with the requirement $E'_e > 10$ GeV, an upper limit on y_{Bj} at 0.6 ensures that the photoproduction background is less than 0.3% of the final event sample. Non-diffractive contributions are suppressed by requiring $x_{I\!P} < 0.025$ and a lower cut on M_X of 3 GeV excludes contributions from diffractive vector meson production. The kinematic selections are summarised in Table 1. In addition, the fact that no part of the system Y is detected in the forward detectors restricts $M_Y \lesssim 1.6$ GeV and $|t| \lesssim 1$ GeV^2, although these variables cannot be reconstructed directly.

The final event sample consists of 3760 events, corresponding to an integrated luminosity of 1.96 pb^{-1}.

The multiplicity analysis is based on charged particles only. Only tracks observed by the central tracking detector, which are successfully fitted to the primary event vertex, contribute to the multiplicity. The multiplicity distribution is determined with an iterative matrix migration

[1] $x_{I\!P} = x_{Bj}/\beta$ with $\beta \approx Q^2/(Q^2 + M_X^2)$; $x_{I\!P}$ is the fractional momentum loss of the initial-state proton and can be interpreted as the fractional momentum of the colour-singlet exchange.

Quantity	Lower limit	Upper limit
Q^2	7.5 GeV^2	100 GeV^2
y_{Bj}	0.05	0.6
$x_{I\!P}$	10^{-4}	0.025
M_X	3 GeV	30 GeV

Table 1: Limits of the kinematical region considered for corrected data.

method based on full Monte Carlo simulation of the detector response [20, 21]. The unfolded distributions do not include the charged decay products of K_S^0, Λ and $\overline{\Lambda}$ and from weakly decaying particles with lifetime large than $8 \cdot 10^{-9}$ s. The target remnant Y is always excluded from the multiplicity.

2.4 Systematic errors

Several sources of possible systematic errors were investigated. For each source the analysis is repeated and the changes in the final results are added in quadrature.

- The error due to the uncertainty of the hadronic energy scale of LAr and BEMC clusters is estimated by changing the scale factors by $\pm 4\%$ and $\pm 20\%$ respectively.
- The systematic uncertainty in the reconstruction of the scattered positron is studied by varying the energy E_e' and angle θ' by $\pm 1\%$ and ± 1 mrad, respectively.
- The influence of the pomeron (reggeon) flux and pomeron (reggeon) structure function used in the Monte Carlo generator for correction is investigated by reweighting the β and $x_{I\!P}$ distributions for Monte Carlo events.
- Both the colour dipole and parton shower models are used to reflect possible influence of the fragmentation model used for correction.
- The track and event selection criteria are varied to estimate remaining backgrounds.
- The convergence criterion for the iterative multiplicity unfolding method is varied to study possible generator dependences of the unfolding procedure.

3 Results

3.1 Charged multiplicity

Figure 3 shows the multiplicity moments of the system X as a function of the invariant mass M_X. The H1 results on the average charged multiplicity $\langle n \rangle$ are compared to measurements of meson diffraction in meson-proton fixed-target experiments [22–24] which extend up to $M_X \approx 15$ GeV. The two data sets agree in the region of overlap. The meson-diffraction data were also found to agree with e^+e^- annihilation results at a CMS energy $\sqrt{s} = M_X$ (after correction for the charged decay products of K^0_S, Λ and $\bar{\Lambda}$, not included in the meson-proton results) and interpreted as evidence [25] that also in meson diffraction a $q\bar{q}$ system is excited. The same conclusion was reached in an analysis of the thrust distribution of the diffractive state [26]. For $M_X > 15$ GeV, no meson-diffractive data exist. In that M_X range, the H1 mean multiplicity is somewhat larger than in e^+e^- induced hadronic final states [27]. The latter are well reproduced by the JETSET model (dotted line) for that process. This model is well-known to adequately account for the features of e^+e^- annihilation discussed here. The RAPGAP model (solid line) agrees with the H1 measurement and reproduces the indication for a stronger growth of $\langle n \rangle$ with M_X than in e^+e^-.

Although the slow rise of the mean multiplicity relative to that of the available phase space is by itself evidence that the diffractive state decays in a string-like manner, with limited transverse momentum along a preferred axis, this measure is too inclusive to reveal finer dynamical details.

Figure 3b,c shows the dispersion, $D = \sqrt{\langle n^2 \rangle - \langle n \rangle^2}$, and the second-order factorial moment of the multiplicity distribution. The latter is defined as $R_2 = \tilde{R}_2 / \langle n \rangle^2$ with

$$\tilde{R}_2 = \langle n(n-1) \rangle = \sum_n P_n \, n(n-1), \tag{1}$$

which is directly linked to the two particle rapidity density through

$$\tilde{R}_2 = \int_\Delta \rho_2(y_1, y_2) \; dy_1 dy_2, \tag{2}$$

where Δ is the considered region in rapidity space. Here P_n is the probability to observe n charged particles. These quantities are measures of the correlations among the produced hadrons [21].

The dispersion D and second factorial moment R_2 for diffractive events in H1 overlap with the meson-diffractive data but are significantly larger than predicted by the JETSET Monte Carlo model [18] for e^+e^-, giving the first indication for stronger multiplicity fluctuations and correlations in diffractive DIS for M_X above ~ 10 GeV. These features are reproduced by the RAPGAP model.

The moments of the multiplicity distributions for particles with positive rapidity and negative rapidity ("forward" and "backward" hemisphere, respectively) are shown separately in Fig. 4. Rapidity is calculated in the $\gamma^* I\!P$ rest system with the positive longitudinal momentum axis taken to be the γ^* direction. The H1 data show no evidence for an asymmetry between forward and backward hemispheres, in contrast to the non-diffractive $\gamma^* p$ mean multiplicity (EMC [28] where the influence of proton fragmentation is known to be substantial. The differences with e^+e^- results, observed in full phase space, are also evident here.

Fig. 5 shows the particle density as a function of rapidity for several values of M_X. The overall symmetrical spectrum rises with M_X in the central region and a rapidity plateau develops.

These features are unambiguous evidence that the diffractive system hadronizes in a jet-like manner with limited transverse momentum along the γ^* axis [26, 29, 30], both in the forward and backward regions. The particle density is also larger in the diffractive DIS than in μN interactions with values of W close to M_X and than in e^+e^- annihilation[2]. This is further illustrated in Fig. 6 where the evolution with M_X ($\sqrt{s}$, W, respectively) of the rapidity density at $y = 0$ ($-0.5 < y < 0.5$) for DDIS is compared with that in other processes including non-diffractive meson-proton collisions [31].

This data comparison suggests that the hadronisation in DDIS final states is quite different from that of a single quark-antiquark, quark-diquark (or two-string) topology as envisaged for the other lepton-induced (meson-induced) processes. As is also the case for the multiplicity moments, the RAPGAP model [13], provides an adequate description of the H1 data.

The single hemisphere KNO distributions [34] show the quantity $\psi(z) = \langle n\rangle P_n$ plotted as a function of the normalized multiplicity $z = n/\langle n\rangle$. The function $\psi(z)$ is expected, and has been observed, to become energy independent at large energies. Here, the KNO distributions are plotted for similar centre-of-mass energies in e^+e^- annihilation and H1 diffractive events, indicating a fair agreement at $\sqrt{s} = 22.5$ GeV, although the multiplicity distribution may be somewhat broader in diffractive DIS at lower energy.

3.2 Forward-Backward Correlations

Many experiments have studied correlations between the charged multiplicities in opposite event hemispheres, known as forward-backward (F-B) multiplicity correlations. These correlations are expected to be sensitive to details of the fragmentation process. The hemispheres are defined by the plane normal to an axis in the centre of mass frame chosen to be the thrust or sphericity axis in e^+e^- annihilation or the beam axis in hadron collisions, and the virtual boson nucleon direction in the hadronic centre of mass in non-diffractive DIS. Here, the axis is made to coincide with the direction of the virtual photon in the $\gamma^* I\!P$ rest system.

In most experiments, the F-B correlation is analysed by studying the regression between the forward multiplicity, n_F, and the backward multiplicity, n_B, which can be expressed as the dependence on n_B of the average number of charged particles in the forward hemisphere $\langle n_F\rangle$ or vice versa. The correlation is usually well parametrised by a simple linear dependence

$$\langle n_F\rangle = a + b \cdot n_B, \tag{3}$$

where b measures the correlation strength.

In e^+e^- annihilation, weak, positive and approximately energy independent F-B correlations have been measured between $\sqrt{s} = 14$ GeV and 46.8 GeV with $b \sim 0.085$ between 14–34.8 GeV [27]. The HRS collaboration, on the other hand, finds no correlations in a high-statistics sample of 2-jet events selected by cuts on sphericity and aplanarity [35]. At LEP, DELPHI [36] has reported a positive F-B correlation ($b = 0.118 \pm 0.009$) comparable to

[2]The e^+e^- JETSET rapidity distributions are calculated with respect to the initial $q\bar{q}$ direction in the CMS.

that at the highest PETRA energy. These results were confirmed by OPAL [37] who measure $b = 0.103 \pm 0.007$. OPAL finds that the small but positive correlation observed at LEP energies in an inclusive sample is primarily a consequence of the superposition of events with distinct numbers of jets and, therefore, different average charged multiplicity. Sub-classes of n-jet events ($n > 2$) show no or even negative F-B correlations.

Results from EMC [28] show no evidence for F-B correlations in μp collisions in the hadronic center of mass energy range $4 < W < 20$ GeV. A similar observation is made in νp and $\bar{\nu} p$ reactions [38].

These data lead to the conclusion that F-B correlations are essentially absent in collisions dominated by single colour-string configurations, including those with hard jets.

The above findings are corroborated by abundant data from hadron interactions, compiled in [39], which cover the energy interval $10 \leq \sqrt{s} \leq 900$ GeV. Over this wide energy range, the F-B correlation strength increases logarithmically with energy and reaches a value $b = 0.65 \pm 0.01$ at $\sqrt{s} = 900$ GeV. The effect has been explained within the framework of the multi-chain Dual-Parton model [40]. The energy dependence and the size of the F-B correlations are, in this approach, directly related to the event-to-event fluctuation in the number of exchanged cut pomerons. Events with n cut pomerons have n-times larger multiplicity density in the central region than that from a single cut pomeron [41]. It may be concluded that F-B correlations in inclusive samples of hadron-collision events arise from the superposition of event sub-samples with distinct particle densities.

Forward-backward correlations have, to the best of our knowledge, not previously been measured in diffractively produced hadron final states. Due to the limited statistics presently available, we have not employed a two-dimensional matrix-unfolding technique used in other works [27, 36, 37] to unfold forward and backward multiplicity distributions simultaneously. Instead, the fully corrected F-B correlation strength is estimated from the separately unfolded and corrected multiplicity distributions in full phase space, in the forward and in the backward hemispheres. Exploiting the relation between the dispersions for the full phase space (D) and for the forward and backward hemispheres (D_F and D_B), one can define the correlation parameter ρ as

$$\rho = \frac{D^2 - D_F^2 - D_B^2}{2 D_F D_B}. \tag{4}$$

The parameter ρ is identical to the slope b in Eqn. (3) [39], in case of forward-backward symmetric systems .

Fig. 8a shows the parameter ρ in two intervals of M_X. The inner (full) error bars represent the statistical (statistical and systematic in quadrature) uncertainties. Also shown are e^+e^- TASSO data, EMC μp data [28] and the NA22 measurement for non-diffractive $\pi^+ p$ collisions at $\sqrt{s} = 22$ GeV [39]. In spite of the large statistical and systematic errors, there is a tendency for stronger correlation in the H1 than in the e^+e^- and μp data. The meson-proton result shows a comparable correlation strength and is significantly larger than in e^+e^-. The JETSET model for e^+e^- (dotted line) reproduces well the TASSO measurements and predicts a negligible effect below $\sqrt{s} = 10$ GeV. The RAPGAP model (solid line) agrees with the H1 measurement. The large difference between this DDIS model and JETSET illustrates the sensitivity of the F-B correlation to differences of dynamics in the two processes and can be exploited in future larger-statistics analyses.

Fig. 8b shows measurements of ρ in asymmetrical rapidity intervals where the acceptance of the H1 detector is high everywhere.

The data can also be qualitatively understood in a picture where, in the proton rest-frame, hadronic fluctuations (light cone Fock states) of the virtual photon interact with the target in a hadron-like fashion [42, 43, 7, 6, 8, 44]. The lowest-order ("aligned jet" [42]) excitation ($\gamma^* \to q\bar{q}$) is dominant at large $\beta \approx Q^2/(M_X^2 + Q^2)$ and can be expected to lead to a similar final state as in e^+e^- annihilation. Higher-order fluctuations (such as $\gamma^* \to q\bar{q}g$ where the gluon has low momentum) dominate at smaller values of β and act as an effective colour-singlet octet-octet dipole [7], corresponding to a boson-gluon fusion subprocess. Due to the larger colour charge at the dipole end-points, such a system hadronises with significantly larger hadron density in the central region of the rest frame of X than a triplet-triplet colour-singlet state [45].

Since the data presented here span rather wide intervals of M_X and are further integrated over Q^2, they are to be interpreted as resulting from an admixture of virtual photon states with quite distinct topological and colour structures. The observation of larger particle density and multiplicity fluctuations, in comparison to single-string dominated data, besides the possible presence of strong forward-backward correlations, proves that the contribution from higher-order Fock states is important. A large contribution from such states is also required to explain the size and the evolution of the diffractive as well as the total virtual-photon proton cross section at very small Bjorken-x [6, 7].

4 Summary

The results presented in this paper show that, although the total average multiplicity is quite similar, the dispersion and second factorial moment of the multiplicity distribution are larger in diffractive DIS than in e^+e^- annihilations. Also the particle density in the central rapidity region of the $\gamma^* I\!P$ center of mass system and possibly the size of the long-range correlation between hadrons in separate hemispheres, is larger in diffractive DIS. This proves that the partonic configuration and colour topology in the system X is more complex than that of a single colour string. The data agree very well with models which assume that the diffractive process is initiated by the interaction of a point-like virtual photon with a gluon-dominated colour-singlet object emitted from the proton, as obtained from a QCD analysis of the diffractive structure function. The dipole picture of virtual photon dissociation offers a complementary explanation of the results.

Acknowledgements

We are grateful to the HERA machine group whose outstanding efforts made this experiment possible. We thank the engineers and technicians for their work in constructing and now maintaining the H1 detector, our funding agencies for financial support, the DESY technical staff for continual assistance, and the DESY directorate for the hospitality they extend to the non-DESY members of the collaboration.

References

[1] ZEUS Collaboration, M. Derrick *et al.*, Phys. Lett. **B315** (1993) 481.

[2] H1 Collaboration, T. Ahmed *et al.*, Nucl. Phys. **B429** (1994) 477.

[3] H1 Collaboration, T. Ahmed *et al.*, Phys. Lett. **B348** (1995) 681.

[4] ZEUS Collaboration, M.Derrick *et al.*, Z. Phys. **C70** (1996) 391.

[5] G. Bertsch, S. J. Brodsky, A. S. Goldhaber and J. G. Gunion, Phys. Rev. Lett. **47** (1981) 297.

[6] W. Buchmüller and A. Hebecker, Phys. Lett. **B355** (1995) 573; A. Edin, G. Ingelman and J. Rathsman, Phys. Lett. **B366** (1996) 371, `hep-ph/9508386`; W. Buchmüller, M. F. McDermott and A. Hebecker, DESY 96–126, `hep-ph/9607290`.

[7] N. N. Nikolaev and B. G. Zakharov, Z. Phys. **C49** (1991) 607; Z. Phys. **C64** (1994) 631.

[8] S. Brodsky, P. Hoyer and L. Magnea, Phys. Rev. **D55** (1997) 5585.

[9] H. Abramowicz, L. Frankfurt, M. Strikman, Surveys in High Energy Physics **11** (1997) 51.

[10] H1 Collaboration, I. Abt *et al.*, Nucl. Instr. and Meth. **A386** (1997) 310 and Nucl. Instr. and Meth. **A386** (1997) 348.

[11] H1 BEMC Group, J. Ban *et al.*, Nucl. Instr. and Meth. **A372** (1996) 399.

[12] H1 Calorimeter Group, B. Andrieu *et al.*, Nucl. Instr. and Meth. **A336** (1993) 460.

[13] H. Jung, Comp. Phys. Comm. **86** (1995) 147.

[14] H1 Collaboration, C. Adloff *et al.*, *Inclusive Measurement of Diffractive Deep-Inelastic ep Scattering*, to be published.

[15] M. Glück, E. Reya and A. Vogt, Z. Phys. **C53** (1992) 651.

[16] L. Lönnblad, Comp. Phys. Comm. **71** (1992) 15.

[17] G. Ingelman, Proceedings of the 1991 Workshop on Physics at HERA, DESY, Vol. 3 (1992) 1366.

[18] T. Sjöstrand, Comp. Phys. Comm. **82** (1994) 74.

[19] A. Kwiatkowski, H. Spiesberger and H.-J. Möhring, Comp. Phys. Comm. **69** (1992) 155.

[20] P. Van Mechelen, H1 internal note 10/96–496.

[21] H1 Collaboration, S. Aid *et al.*, Z. Phys. **C72** (1996) 573.

[22] F.C. Winkelmann *et al.*, Phys. Rev. Lett. **32** (1974) 121.

[23] R.L. Cool *et al.*, Phys. Rev. Lett. **48** (1982) 1451.

[24] NA22 Collaboration, M. Begalli *et al.*, Z. Phys. **C55** (1992) 531.

[25] S.P. Misra, A.R. Panda and B.K. Parida, Phys. Rev. Lett. **45** (1980) 322.

[26] NA22 Collaboration, M. Adamus *et al.*, Z. Phys. **C39** (1988) 301.

[27] TASSO Collaboration, W. Braunschweig *et al.*, Z. Phys. **C45** (1989) 193.

[28] EMC Collaboration, M. Arneodo *et al.*, Nucl. Phys. **B258** (1985) 249.

[29] UA4 collaboration, D. Barnard *et al.*, Phys. Lett. **B166** (1986) 459.

[30] UA5 Collaboration, R. E. Ansorge *et al.*, Z. Phys. **C33** (1986) 175.

[31] NA22 Collaboration, M. Adamus *et al.*, Z. Phys. **C37** (1988) 215.

[32] EMC Collaboration, M. Arneodo *et al.*, Z. Phys. **C35** (1987) 335.

[33] E665 Collaboration, M. R. Adams *et al.*, Z. Phys. **C61** (1994) 179.

[34] Z. Koba, H. B. Nielsen and P. Olesen, Nucl. Phys. **B40** (1972) 317.

[35] HRS Collaboration, M. Derrick *et al.*, Phys. Rev. **D34** (1986) 3304; Z. Phys. **C35** (1987) 323.

[36] DELPHI Collaboration, P. Abreu *et al.*, Z. Phys. **C50** (1991) 185.

[37] OPAL Collaboration, R. Akers *et al.*, Phys. Lett. **B320** (1994) 417.

[38] H. Grässler *et al.*, Nucl. Phys. **B223** (1983) 269.

[39] NA22 Collaboration, V. V. Aivazyan *et al.*, Z. Phys. **C42** (1989) 533.

[40] A. Capella and J. Tran Thanh Van, Z. Phys. **C18** (1983) 85; A. Capella and A. Krzywicki, Phys. Rev. **D18** (1978) 4120.

[41] V.A. Abramovskii, V.N. Gribov, O.V. Kancheli, Yad. Fiz. **18** (1973) 595; Sov. J. Nucl. Phys. **18** (1974) 308.

[42] J.D. Bjorken, AIP Conference Proceedings No. 6, Particles and Fields Subseries No. 2, Ed. M. Bander, G. Shaw and D. Wong (AIP, New York, 1972); J.D. Bjorken and J. Kogut, Phys. Rev. **D8** (1973) 1341.

[43] J.D. Bjorken, *Rapidity Gaps in QCD*, preprint SLAC–PUB–7096 (1996), `hep-ph/9601363`.

[44] A. Białas, Acta Phys. Pol. **B27** (1996) 1263.

[45] M. Wüsthoff, *Large Rapidity Gap Events in Deep-Inelastic Scattering*, ANL-HEP-PR-97-03, `hep-ph/9706407`.

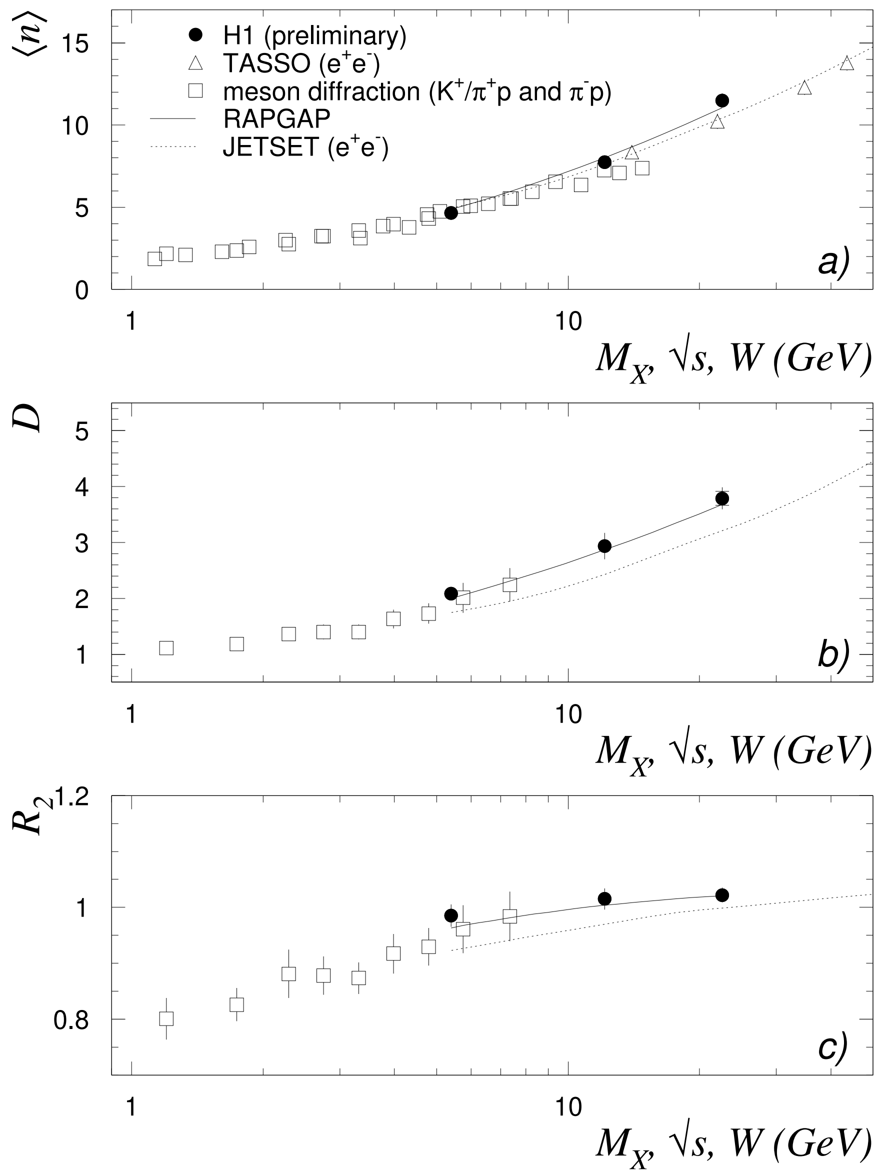

Figure 3: Multiplicity moments $\langle n \rangle$, D and R_2 as a function of centre-of-mass energy (M_X, $\sqrt{s}$, W). The H1 and RAPGAP points are computed from the charged particle multiplicity of the full system X. The TASSO [27], meson-diffraction [24, 25] and JETSET points reflect the multiplicity structure of the full event.

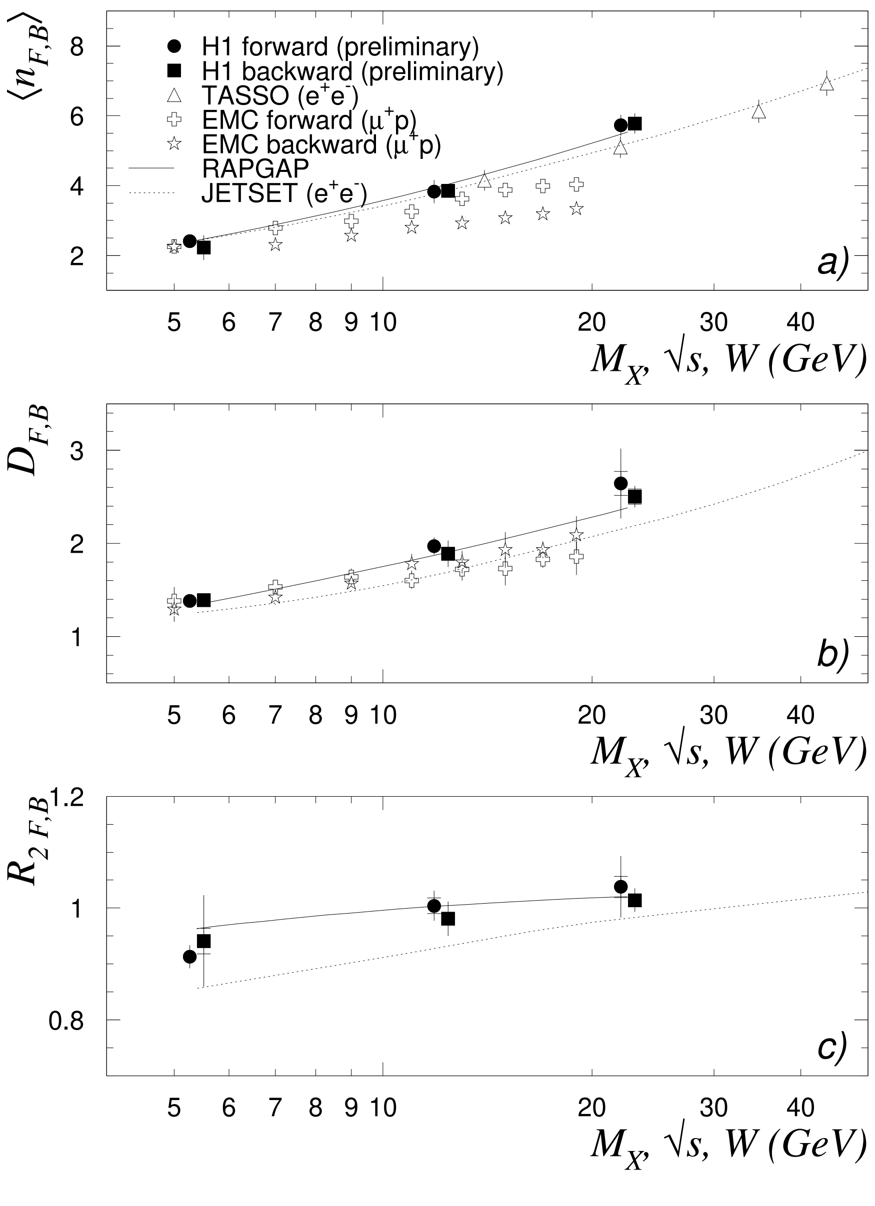

Figure 4: Same as in Fig. 3, but for the forward and backward hemispheres separately. For clarity, the H1 data points are slightly offset along the horizontal axis. EMC data points are taken from [28].

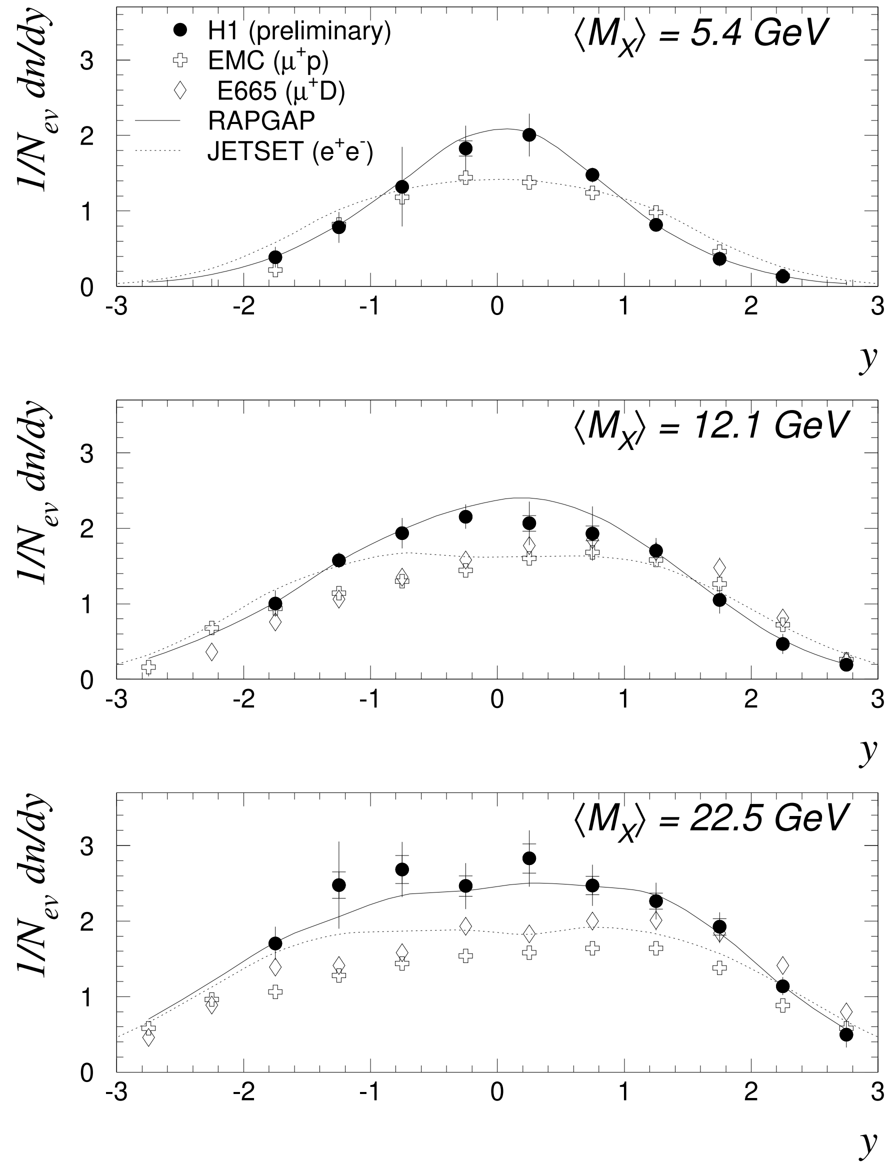

Figure 5: Particle density as function of rapidity y for three values of M_X. In the rest frame of X, the reference axis is the $\gamma^* I\!P$ axis with the positive z-axis defined by the photon direction. The JETSET predictions are obtained w.r.t. the $q\overline{q}$ axis. For H1, RAPGAP and JETSET, the M_X or $\sqrt{s}$ values are as indicated. For EMC [32], the three W values are 5.2, 11.0 and 19.0 GeV, respectively. The E665 [33] data were obtained for $W = 11.4$ and 23.6 GeV.

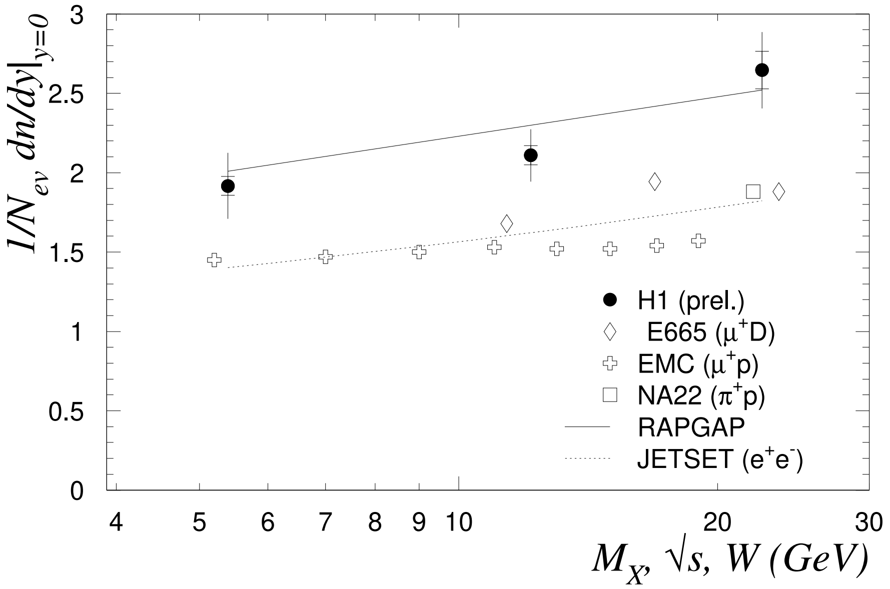

Figure 6: A comparison of the charged particle density in a central rapidity region ($-0.5 < y < 0.5$) as a function of centre-of-mass energy. The NA22 data point is for non-diffractive π^+p collisions [31].

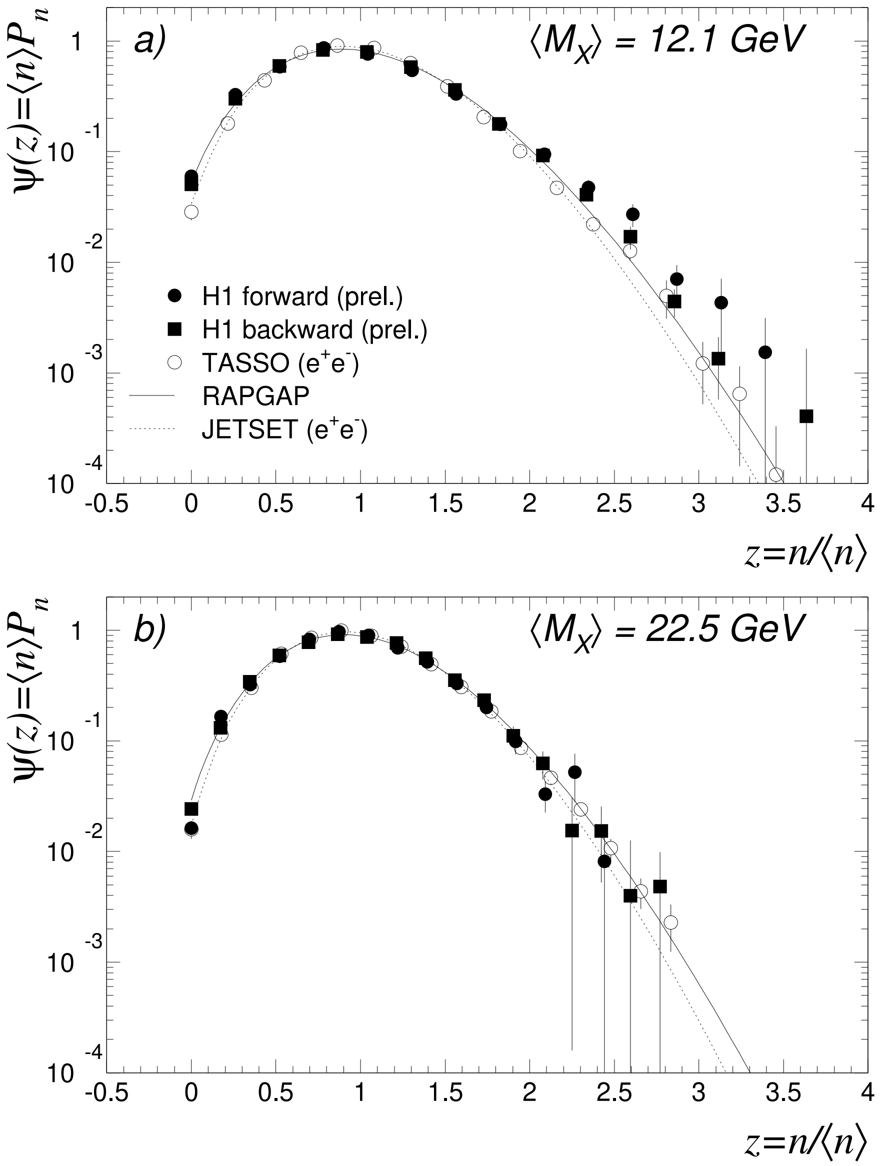

Figure 7: Single hemisphere multiplicity distributions in KNO-form for two values of M_X. The TASSO [27] points at $\sqrt{s} = 14$ and 22 GeV include decay products of K_S^0, Λ and $\overline{\Lambda}$.

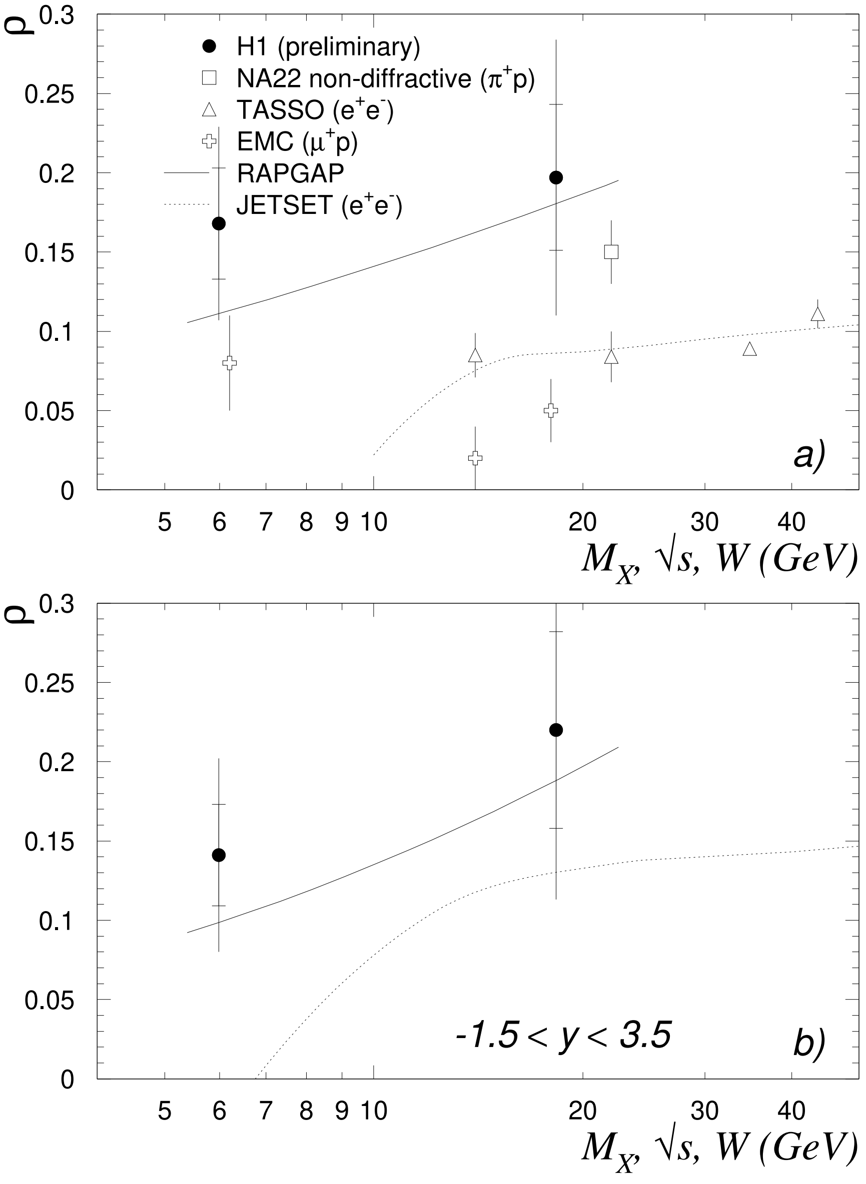

Figure 8: The parameter ρ, which reflects the correlation between the number of particles in forward and backward hemispheres, as a function of centre-of-mass energy. The lower plot was obtained for a region in rapidity where acceptance corrections are small.